Mon. Not. R. Astron. Soc. **298,** 387–394 (1998)

Local stellar kinematics from *Hipparcos* data

Walter Dehnen and James J. Binney
Theoretical Physics, 1 Keble Road, Oxford OX1 3NP

Accepted 1998 March 9. Received 1998 February 4; in original form 1997 October 9

ABSTRACT

From the parallaxes and proper motions of a kinematically unbiased subsample of the *Hipparcos* Catalogue, we have re-determined as a function of colour the kinematics of main-sequence stars.

Whereas the radial and vertical components of the mean heliocentric velocity of stars show no trend with colour, the component in the direction of Galactic rotation nicely follows the asymmetric drift relation, except for stars bluer than $B-V=0.1$ mag. Extrapolating to zero dispersion yields, for the velocity of the Sun with respect to the local standard of rest (LSR) in $\mathrm{km\,s^{-1}}$, $U_0 = 10.00 \pm 0.36$ (radially inwards), $V_0 = 5.25 \pm 0.62$ (in the direction of Galactic rotation) and $W_0 = 7.17 \pm 0.38$ (vertically upwards).

Parenago's discontinuity is beautifully visible in a plot of velocity dispersion against colour: the dispersion, which is essentially constant for late spectral types, decreases towards early spectral types blueward of $B-V \approx 0.61$ mag.

We determine the velocity dispersion tensor $\boldsymbol{\sigma}^2$ as function of colour. The mixed moments involving vertical motion are zero within the errors, while σ_{xy}^2 is non-zero at about $(10\,\mathrm{km\,s^{-1}})^2$ independently of colour. The resulting vertex deviations are about 20° for early-type stars and $10° \pm 4°$ for old-disc stars. The persistence of the vertex deviation to late-type stars implies that the Galactic potential is significantly non-axisymmetric at the solar radius. If spiral arms are responsible for the non-axisymmetry, they cannot be tightly wound.

Except for stars bluer than $B-V=0.1$ mag, the ratios of the principal velocity dispersions are given by $\sigma_1{:}\sigma_2{:}\sigma_3 \approx 2.2:1.4:1$, while the absolute values increase with colour from $\sigma_1 \approx 20\,\mathrm{km\,s^{-1}}$ at $B-V=0.2$ mag to $\sigma_1 \approx 38\,\mathrm{km\,s^{-1}}$ at Parenago's discontinuity and beyond. These ratios imply significant heating of the disc by spiral structure and that $R_0/R_\mathrm{d} \simeq 3$ to 3.5, where R_d is the scalelength of the disc.

Key words: stars: kinematics – Galaxy: fundamental parameters – Galaxy: kinematics and dynamics – solar neighbourhood – Galaxy: structure.

1 INTRODUCTION

The kinematics of stars near the Sun has long been known to provide crucial information regarding both the structure and the evolution of the Milky Way. Karl Schwarzschild (1908) already interpreted the distribution of random velocities as forming a triaxial 'velocity ellipsoid', which Oort, B. Lindblad and Strömberg were able to relate to the large-scale structure of the disc. In the early 1950s Parenago (1950), Nancy Roman (1950, 1952) and others pointed out that stellar kinematics varies systematically with stellar type, in the sense that groups of stars that are on average younger have smaller velocity dispersions and larger mean Galactic rotation velocities than older stellar groups. Spitzer & Schwarzschild (1953), Barbanis & Woltjer (1967) and Wielen (1977) explained these correlations in terms of the diffusion of stars through phase space as the Galactic disc ages – for recent studies of these processes see Binney & Lacey (1988) and Jenkins (1992).

The *Hipparcos* Catalogue ESA 1997 provides an important opportunity to re-examine the fundamental data of solar neighbourhood kinematics by providing the first all-sky catalogue of *absolute* parallaxes and proper motions. From the *Hipparcos* Catalogue we can, moreover, extract samples that are completely free of the kinematic biases that have plagued similar studies in the past. Binney et al. (1997) obtained some preliminary results from a sample of 5610 stars around the South Celestial Pole. Here we extend these results in three ways.

(i) We have joined the relatively deep sample of Binney et al. (1997) to a sample that covers the whole sky but has a significantly brighter limiting magnitude. The combined sample gives significantly better statistics for earlier spectral types.

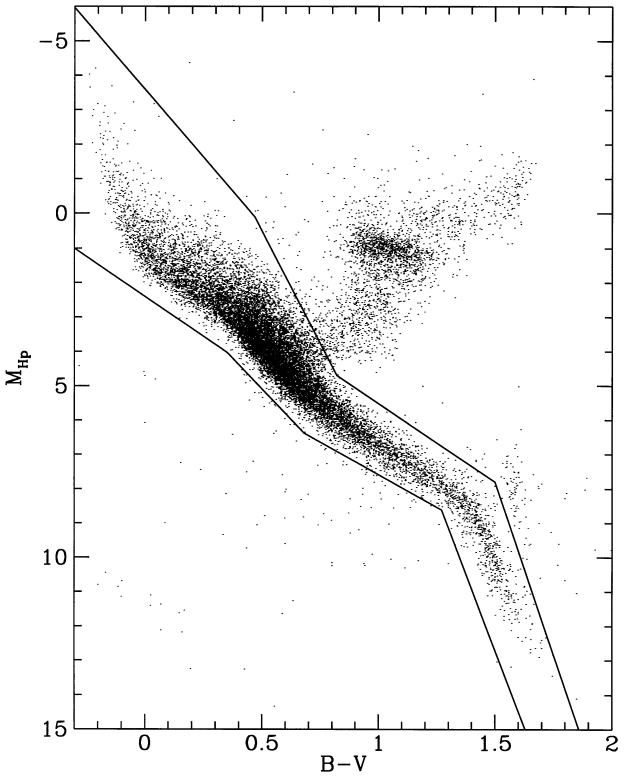

Figure 1. Hertzsprung–Russell diagram (M_{Hp} is the absolute magnitude in *Hipparcos*'s own passband) of the 18 860 single *Hipparcos* stars with relative parallax errors less than 10 per cent. The lines are used to select the main sequence and have 16 054 stars between them.

(ii) Since we now have some all-sky coverage we are able to impose a stricter limit on parallax errors: we use only stars with $\sigma_\pi/\pi \leq 0.1$, whereas Binney et al. accepted stars with $\sigma_\pi/\pi \leq 0.2$.

(iii) Whereas Binney et al. only reported the solar motion and a single estimate of random velocity for each spectral type, we derive the lengths of the axes of the velocity ellipsoid and analyse its orientation.

Section 2 describes the new sample. Section 3 explains how we have analysed the sample. Section 4 gives the results, and Section 5 discusses them.

2 THE SAMPLE

Our sample has to meet several criteria if it is accurately to determine local stellar kinematics as a function of stellar age. First, it must be kinematically unbiased, i.e. faithfully represent at each point in the Hertzsprung–Russell diagram the kinematics of all nearby stars. Secondly, it should be confined to main-sequence stars, since only for these is there a one-to-one relation between age and either colour or absolute luminosity. Thirdly, it should be based on accurate astrometry, and, fourthly, it should contain no multiple stars because their kinematics contains additional motions.

We ensured satisfaction of the last two criteria by taking only single stars with relative parallax errors smaller than 10 per cent. This is small enough that the non-linear dependence of tangential velocity on parallax does not create a strongly skewed distribution of tangential velocity errors, which would greatly complicate the analysis. A 10 per cent parallax error cut-off automatically excludes remote stars, and leaves just 18 860 of the 118 218 stars in the *Hipparcos* Catalogue. The Hertzsprung–Russell diagram of the selected stars is shown in Fig. 1, which also shows the division lines that we used to select main-sequence stars; there are 16 054 stars between these lines. However, given the very heterogeneous nature of the *Hipparcos* Catalogue, they almost certainly do not comprise a kinematically unbiased sample. The only reliable way to extract such a sample is to isolate a magnitude-limited subsample.

According to its vol I, p. 4, the *Hipparcos* Catalogue comprises some 60 000 objects complete to about 7.3 to 9 mag depending on Galactic latitude, b, and stellar type. Actually, however, 59 stars brighter than $V_T = 7.0$ (the subscript T denotes the passbands used by Tycho, the starmapper of *Hipparcos*) are absent from the Catalogue (see the table on p. 142 of vol. I). We used the Tycho Catalogue ESA 1997, which is essentially complete to 11 mag, to construct an almost complete subsample of *Hipparcos* stars. For each of $16 \times 16 \times 10$ uniformly spaced bins in $\sin b$, Galactic longitude, ℓ, and $B_T - V_T$, we took all *Hipparcos* stars brighter (in V) than the second brightest star per bin that is contained in the Tycho but not the *Hipparcos* Catalogue. This gives a subsample with 95 per cent completeness (as compared with the Tycho Catalogue) and 47 558 stars (compared with 60 000 claimed), of which 10 706 have $\sigma_\pi/\pi \leq 0.1$ and lie between the lines in Fig. 1.

Another kinematically unbiased subsample is given by *Hipparcos* Proposal 018: all stars spectrally classified in the Michigan Catalogues by 1982 (Houk & Cowley 1975; Houk 1978, 1982) that, judged from their spectral classification, should be within 80 pc from the Sun – this 'SCP' sample is the one analysed by Binney et al. (1997). It contains 6845 stars south of $\delta = -28°$ (covering 26.5 per cent of the sky), of which 3172 are single and have $\sigma_\pi/\pi \leq 0.1$ and lie between the lines in Fig. 1.

Whereas most of the stars in the all-sky sample are of early type and intrinsically luminous, the SCP sample contains many late-type dwarfs. The union of the samples is kinematically unbiased and has 11 865 entries. It is this combined sample that we analyse below. Fig. 2 shows its Hertzsprung–Russell diagram.

3 ANALYSIS TECHNIQUE

Hipparcos provides us with parallax measurements of unprecedented accuracy, and proper motions the accuracy of which is only comparable to that of ground-based astrometry on account of the short duration (3.3 yr) of the *Hipparcos* mission. Unfortunately, the *Hipparcos* astrometry mission was not complemented by a programme to measure the radial velocities of the same stars, so we do not know the space velocities of most sample stars. As Binney et al. (1997) have demonstrated, the stars with known radial velocities form a kinematically biased subsample. Hence we have to discard the known radial velocities and work with the *Hipparcos* data alone.

3.1 The projection equation

The velocity of a star relative to the Sun can be divided into three components: (i) the peculiar velocity of the star, (ii) that of the Sun, and (iii) the contribution from Galactic rotation. Here we are dealing with the first two parts, and correct for Galactic rotation before further analysis. Given observed values $\mu_\ell^{(\rm obs)}$ and $\mu_b^{(\rm obs)}$, the corrected values are

$$\begin{aligned} \mu_\ell &= \mu_\ell^{(\rm obs)} - A\cos(2\ell) - B, \\ \mu_b &= \mu_b^{(\rm obs)} + A\sin(2\ell)\cos b \sin b. \end{aligned} \tag{1}$$

We used the values of A and B derived by Feast & Whitelock

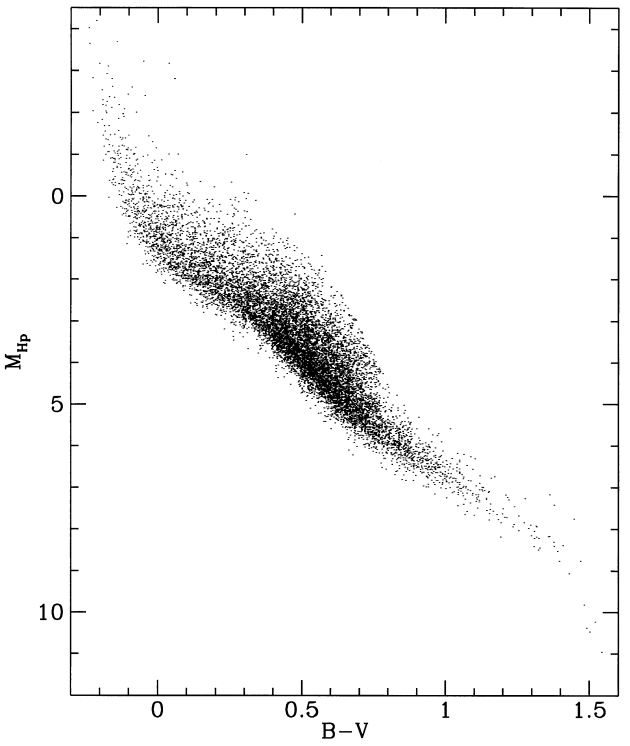

Figure 2. Hertzsprung–Russell diagram for the stars in our kinematically unbiased sample of 11 865 single main-sequence stars.

(1997) from *Hipparcos* Cepheids: $A = 14.82\,\mathrm{km\,s^{-1}\,kpc^{-1}}$ and $B = -12.37\,\mathrm{km\,s^{-1}\,kpc^{-1}}$.

Let us introduce a Cartesian coordinate system such that $\hat{\boldsymbol{x}}$ points towards the Galactic Centre, $\hat{\boldsymbol{y}}$ in the direction of Galactic rotation, and $\hat{z}$ towards the North Galactic Pole. We consider a star with parallax π and heliocentric velocity $\boldsymbol{v}$, and define the star's proper motion velocity $\boldsymbol{p}$ to be

$$\boldsymbol{p} \equiv \frac{1\,\mathrm{au}}{\sin\pi}\begin{bmatrix} -\sin\ell\,\cos b\,\mu_\ell - \cos\ell\,\sin b\,\mu_b \\ \cos\ell\,\cos b\,\mu_\ell - \sin\ell\,\sin b\,\mu_b \\ \cos b\,\mu_b \end{bmatrix}. \tag{2}$$

Then $\boldsymbol{p}$ and $\boldsymbol{v}$ are related by

$$\boldsymbol{p} = \mathbf{A}\cdot\boldsymbol{v}, \tag{3}$$

where the matrix $\mathbf{A}$ is defined by

$$\mathbf{A} \equiv \mathbf{I} - \hat{\boldsymbol{r}}\otimes\hat{\boldsymbol{r}}, \tag{4}$$

with $\hat{\boldsymbol{r}}$ the unit vector to the star. $\mathbf{A}$ projects velocities on to the celestial sphere. It is symmetric and, as every projection operator, obeys $\mathbf{A}^2 = \mathbf{A}$ and is singular. Hence we cannot invert (3); we needed the radial velocity to recover $\boldsymbol{v}$.

3.2 The mean motion

The solar motion relative to any given group of stars is simply minus the mean motion of that group with respect to the Sun, $\boldsymbol{v}_\odot = -\langle\boldsymbol{v}\rangle$. For a kinematically unbiased sample of nearby stars we can safely assume that the positions on the sky $\hat{\boldsymbol{r}}$ are uncorrelated with the velocities $\boldsymbol{v}$. With this assumption, taking the sample mean of equation (3) yields $\langle\boldsymbol{p}\rangle = \langle\mathbf{A}\rangle\cdot\langle\boldsymbol{v}\rangle$, which can be inverted to give

$$-\boldsymbol{v}_\odot = \langle\boldsymbol{v}\rangle = \langle\mathbf{A}\rangle^{-1}\cdot\langle\boldsymbol{p}\rangle. \tag{5}$$

It is easy to show that for a group of stars that is isotropically distributed over a celestial hemisphere $\langle\mathbf{A}\rangle = \frac{2}{3}\mathbf{I}$, where the factor $\frac{2}{3}$ arises from the fact that we only know two of the three velocity components for each star. Let us denote the motions relative to the mean by

$$\begin{aligned} \boldsymbol{v}' &\equiv \boldsymbol{v} - \langle\boldsymbol{v}\rangle, \\ \boldsymbol{p}' &\equiv \boldsymbol{p} - \mathbf{A}\cdot\langle\boldsymbol{v}\rangle, \end{aligned} \tag{6}$$

and consider the quantity

$$S^2 \equiv \left\langle|\boldsymbol{p}'|^2\right\rangle. \tag{7}$$

It can be shown that the choice of $\langle\boldsymbol{v}\rangle$ given by (5) minimizes S^2, and (with equations 3 and 4) that

$$S^2 = \left\langle|\boldsymbol{v}'|^2\right\rangle - \left\langle(\boldsymbol{v}'\cdot\hat{\boldsymbol{r}})^2\right\rangle. \tag{8}$$

Hence S^2 is a measure for the velocity dispersion of the group.

3.3 The velocity dispersion tensor

Similarly to the mean velocity, the second-order moments of the space velocities can be inferred. From equation (3) we can obtain

$$\boldsymbol{p}'\otimes\boldsymbol{p}' = (\mathbf{A}\cdot\boldsymbol{v}')\otimes(\mathbf{A}\cdot\boldsymbol{v}') = (\mathbf{A}\otimes\mathbf{A})\cdot(\boldsymbol{v}'\otimes\boldsymbol{v}'). \tag{9}$$

The velocity dispersion tensor $\boldsymbol{\sigma}^2$ is the sample average of $(\boldsymbol{v}'\otimes\boldsymbol{v}')$, so after averaging (9) we can solve for $\boldsymbol{\sigma}^2$, exactly as we did for $\langle\boldsymbol{v}\rangle$ above, and the same holds, in principle, for the velocity moments of higher orders.

However, if we were to solve the expectation of equation (9) for $\boldsymbol{\sigma}^2$, we would in general find that the recovered tensor $\boldsymbol{\sigma}^2$ was not symmetric, because $\langle A_{ij}A_{kl}\rangle \neq \langle A_{kj}A_{il}\rangle$. Since we know a priori that $\boldsymbol{\sigma}^2$ *is* a symmetric tensor, with six rather than nine independent elements, it is advantageous to impose this symmetry by solving

$$\left\langle p'_i p'_k\right\rangle = \tfrac{1}{2}\sum_{jl}\left\langle A_{ij}A_{kl} + A_{kj}A_{il}\right\rangle\,\sigma_{jl}. \tag{10}$$

For the computer this is more conveniently written as $\langle\boldsymbol{u}\rangle = \mathbf{B}\cdot\langle\boldsymbol{s}\rangle$, where $\langle\boldsymbol{u}\rangle$ and $\langle\boldsymbol{s}\rangle$ are vectors containing the six independent components of $\langle p'_i p'_j\rangle$ and σ_{ij}, respectively, whereas $\mathbf{B}$ is the corresponding 6×6 matrix. With this notation the dispersion tensor is estimated via

$$\langle\boldsymbol{s}\rangle = \langle\mathbf{B}\rangle^{-1}\cdot\langle\boldsymbol{u}\rangle. \tag{11}$$

Somewhat surprisingly, for an isotropic sample the matrix $\langle\mathbf{B}\rangle^{-1}$ is not diagonal, in contrast to $\langle\mathbf{A}\rangle^{-1}$. It turns out that the diagonal terms of $\boldsymbol{\sigma}^2$ are coupled. Quantitatively,

$$\begin{pmatrix}\sigma_x^2\\ \sigma_y^2\\ \sigma_z^2\end{pmatrix} = \frac{3}{14}\begin{pmatrix}9 & -1 & -1\\ -1 & 9 & -1\\ -1 & -1 & 9\end{pmatrix}\cdot\begin{pmatrix}\langle p'_x p'_x\rangle\\ \langle p'_y p'_y\rangle\\ \langle p'_z p'_z\rangle\end{pmatrix}, \tag{12}$$

while all other off-diagonal terms of $\langle\mathbf{B}\rangle^{-1}$ average to zero for an isotropic sample.

3.4 Errors

In the equations derived so far, we have ignored the effects of (i) Poisson noise, as well as (ii) systematic and (iii) random uncertainties in the *Hipparcos* data.

3.4.1 Poisson noise

The finite sample size is by far the dominant source of uncertainties in the derived kinematic quantities. The resulting variances for $\langle\boldsymbol{v}\rangle$,

S^2 and $\langle \boldsymbol{s} \rangle$ can be estimated by, respectively,

$$\boldsymbol{V}(\langle \boldsymbol{v} \rangle) = N^{-1} \langle \mathbf{A} \rangle^{-1} \left\langle |\boldsymbol{p}'|^2 \right\rangle, \tag{13}$$

$$V(S^2) = N^{-1} \left(\left\langle |\boldsymbol{p}'|^4 \right\rangle - \left\langle |\boldsymbol{p}'|^2 \right\rangle^2 \right), \tag{14}$$

$$\boldsymbol{V}(\langle \boldsymbol{s} \rangle) = N^{-1} \langle \mathbf{B} \rangle^{-1} \left\langle |\boldsymbol{u} - \mathbf{B}\cdot\boldsymbol{s}|^2 \right\rangle. \tag{15}$$

In Section 4 we only give the diagonal elements of these variance matrices (i.e. the standard errors of the quantities evaluated); the correlations between the parameters are generally very small (a few per cent), except for the diagonal elements of $\boldsymbol{\sigma}^2$, as shown above.

3.4.2 *Systematic errors in the Hipparcos* data

3.4.2.1 Proper motion. The *Hipparcos* reference frame may rotate systematically with respect to inertial space by up to $0.25\,\mathrm{mas\,yr^{-1}}$ (ESA 1997). This corresponds to $\delta v = 0.085\,\mathrm{km\,s^{-1}}$ at the mean stellar distance of 72 pc for our sample.

The apparent tangential velocity induced by this rotation has opposite signs in directions $\hat{\boldsymbol{r}}$ and $-\hat{\boldsymbol{r}}$, and for an isotropic sample no net effect is expected. Anisotropies in our sample are small, of the order of 10 per cent (that is the fraction of stars exclusively from the SCP sample covering a cap around the South Celestial Pole), so the induced error is expected to be less than $0.1\delta v$, i.e. completely negligible.

For the velocity dispersions, there is no cancellation and the effect contributes fully. However, since it adds to σ^2, the resulting error in a dispersion σ is $(\delta v)^2/2\sigma$, i.e. again completely negligible.

3.4.2.2 Parallax. Even though *Hipparcos*'s instrumental configuration and observations were designed to give absolute parallaxes, a systematic error could have been introduced through a certain thermal coupling between the satellite and the solar illumination. In this case, one expects a constant offset $\delta\pi$ limited to be less than 0.1 mas in modulus (Perryman, private communication). Such an offset would imply that the tangential velocities $\boldsymbol{p}$ are systematically too small (large), and with them the derived mean motion and velocity dispersions. To quantify the effect, we will apply our numerical apparatus to the data with the parallaxes artificially raised or lowered by 0.1 mas. The size of the resulting deviations is about a quarter of the uncertainties due to Poisson noise (see Section 4 below).

3.4.3 *Random measurement uncertainties*

The uncertainties in proper motion and parallax are much larger than those in position, which can be ignored for our purposes. Our sample is restricted to stars with parallax errors less than 10 per cent, so we can use simple error propagation and ignore higher-order effects introduced by the non-linear dependence of the velocities on parallax. For the variance $\boldsymbol{V}(\boldsymbol{p})$ of the tangential velocity this gives

$$V_{ij}(\boldsymbol{p}) = \sum_{kl} \frac{\partial p_i}{\partial \xi_k} \frac{\partial p_j}{\partial \xi_l} V_{kl}(\boldsymbol{\xi}), \tag{16}$$

where $\boldsymbol{\xi} \equiv (\pi, \cos\delta\,\mu_\alpha, \mu_\delta)$ are the observed astrometric parameters and $\boldsymbol{V}(\boldsymbol{\xi})$ is their variance, which can be derived from the errors and correlations given in the *Hipparcos* Catalogue.

With knowledge of $\boldsymbol{V}(\boldsymbol{p})$ for all stars, we can obtain corrected values for the dispersions by subtracting the errors in quadrature. The resulting correction terms are

$$\Delta S^2 = \mathrm{Tr}\left[\left\langle \boldsymbol{V}(\boldsymbol{p}') \right\rangle\right], \tag{17}$$

$$\Delta\boldsymbol{\sigma}^2 = \langle \mathbf{B} \rangle^{-1} \cdot \left\langle u[\boldsymbol{V}(\boldsymbol{p}')] \right\rangle, \tag{18}$$

where $u[\boldsymbol{V}]$ denotes the six independent elements of $\boldsymbol{V}$, while

$$\boldsymbol{V}(\boldsymbol{p}') = \boldsymbol{V}(\boldsymbol{p}) + \mathbf{A}\cdot\boldsymbol{V}(\langle \boldsymbol{v} \rangle)\cdot\mathbf{A}, \tag{19}$$

with $\boldsymbol{V}(\langle \boldsymbol{v} \rangle)$ given in equation (13). In the application to the data below, the corrections are less than 1 per cent, as expected for a 10 per cent effect added in quadrature.

The contribution of random measurement uncertainties to the errors is of the order of these corrections divided by the sample size, i.e. negligible compared with the Poisson noise.

4 RESULTS

We will now apply the formulæ from the last section to our sample. The analysis technique relies heavily on taking averages of the various observed kinematic quantities. Unfortunately, averages are sensitive to outliers such as halo stars, and rejection of them is an important issue. Here, we will use an iterative method: in the solution for the various quantities we rejected stars that contribute to S^2 (equation 7) by more than κ^2 times the value of S^2 obtained in the previous iteration. Convergence is usually obtained after a few iterations (or never if κ is too small). The results prove to be insensitive to κ in the range of 3 to 4. Below we used $\kappa = 4$, which led to the rejection of 22 stars (out of 11 865) compared with 7 expected for a Gaussian distribution.

4.1 The solar motion and Parenago's discontinuity

We have binned the stars in $B - V$, such that the bins are no smaller than 0.02 mag and contain no fewer than 500 stars. For each bin, Fig. 3 plots the solar motion with respect to the stars in the bin, $\boldsymbol{v}_\odot = -\langle \boldsymbol{v} \rangle$, and S, which is a measure for the bin's velocity dispersion, versus the mean colour. As usual, U, V and W denote the components of $\boldsymbol{v}_\odot$ in the $\hat{\boldsymbol{x}}$, $\hat{\boldsymbol{y}}$ and $\hat{\boldsymbol{z}}$ directions as defined in Section 3.1. U and W do not vary significantly between bins, while both V and S increase systematically from early to late spectral types. The points in S display very beautifully Parenago's (1950) discontinuity: around $B - V \simeq 0.61$ mag there is an abrupt change in gradient from a strongly positive value to about zero. The same discontinuity is visible, although less clearly, in the data for V. Parenago's discontinuity is thought to arise from the fact that the mean age of stars decreases as one moves blueward of the discontinuity, while it is independent of colour redward of the discontinuity: scattering processes cause the random velocities of stars to increase steadily with age (e.g. Jenkins 1992). Hence velocity dispersion reflects age, and decreases as one moves blueward from the discontinuity through ever younger stellar groups, while remaining constant with mean age redward of the discontinuity. The discontinuity itself should occur at the colour for which the main-sequence lifetime of a star equals the age of the Galactic disc. However, since stars change colour during their life on the main sequence, detailed modelling of stellar populations is necessary, to infer the age of the stellar disc from this datum (Binney & Dehnen, in preparation).

4.2 The Sun's velocity with respect to the LSR

Fig. 4 is a plot of U, V and W versus S^2. For $S \gtrsim 15\,\mathrm{km\,s^{-1}}$, this clearly shows the linear dependence of V on S^2 that is predicted by

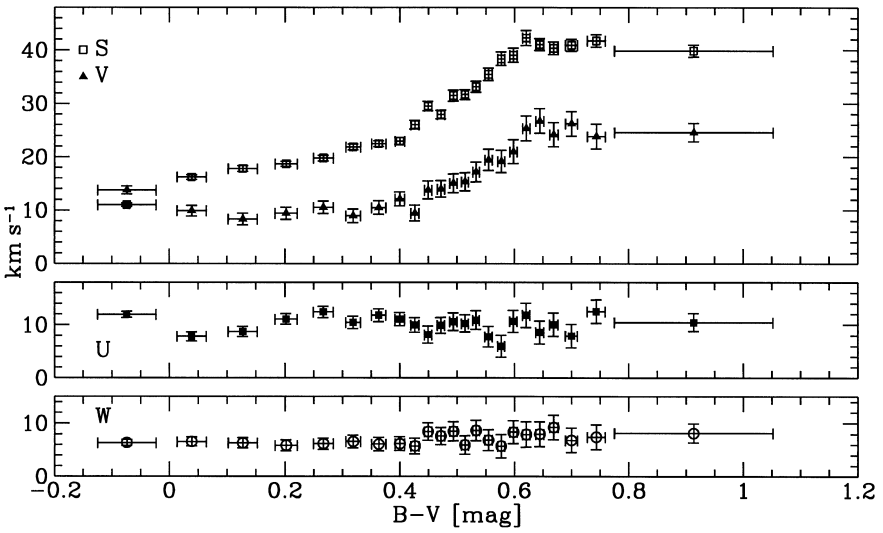

Figure 3. The components U, V and W of the solar motion with respect to stars with different colour $B-V$. Also shown is the variation of the dispersion S with colour.

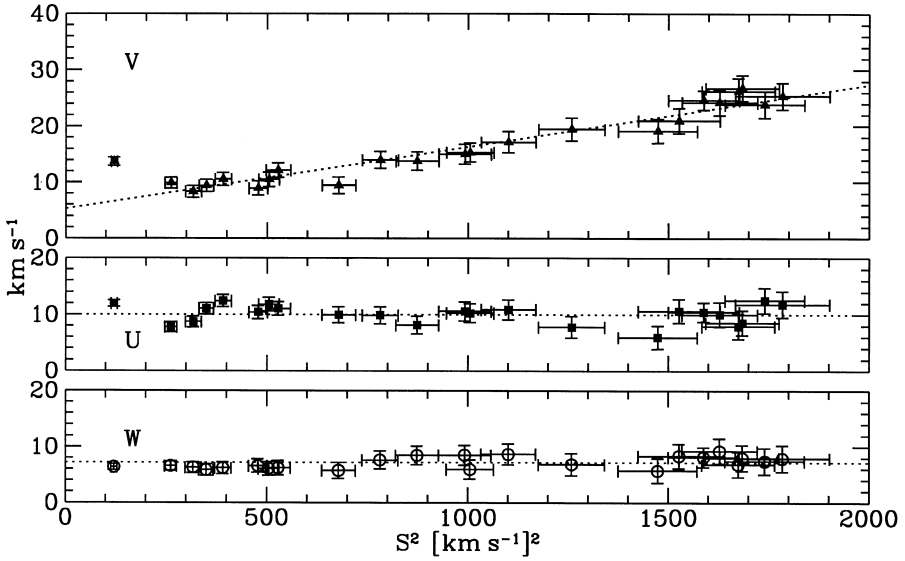

Figure 4. The dependence of U, V and W on S^2. The dotted lines correspond to the linear relation fitted (V) or the mean values (U and W) for stars bluer than $B-V=0$.

Strömberg's asymmetric drift equation [e.g. equation (4-34) of Binney & Tremaine (1987, hereafter BT)]. That is, V increases systematically with S^2 because the larger a stellar group's velocity dispersion is, the more slowly it rotates about the Galactic Centre and the faster the Sun moves with respect to its lagging frame.

For very early-type stars with $B-V \lesssim 0.1$ mag and/or $S \lesssim 15\,\mathrm{km\,s^{-1}}$, the V-component of $\langle \boldsymbol{v} \rangle$ decreases with increasing S, colour, and hence age contradicting the explanation given in the last paragraphs. However, the stars concerned are very young, and there are several possibilities for them not to follow the general trend. First, because of their youth these stars are unlikely to constitute a kinematically well-mixed sample; rather, they move close to the orbit of their parent cloud; many will belong to a handful of moving groups. Secondly, Strömberg's asymmetric drift relation predicts a linear relation between V and S^2 only if both the shape of the velocity ellipsoid, i.e. the ratios of the eigenvalues of $\boldsymbol{\sigma}$, and the radial density gradient are independent of S. Young stars probably violate these assumptions, especially the latter one.

The radial and vertical components U_0 and W_0 of the velocity of the Sun with respect to the LSR (the velocity of the closed orbit in the plane that passes through the location of the Sun) can be derived from $\langle \boldsymbol{v} \rangle$ estimated for all stars together. The component in the direction of rotation, V_0, may be read off from Fig. 4 by linearly extrapolating back to $S=0$. Ignoring stars blueward of $B-V=0$ mag we find

$$\begin{aligned} U_0 &= 10.00 \pm 0.36 \quad (\pm 0.08) \quad \mathrm{km\,s^{-1}}, \\ V_0 &= 5.25 \pm 0.62 \quad (\pm 0.03) \quad \mathrm{km\,s^{-1}}, \\ W_0 &= 7.17 \pm 0.38 \quad (\pm 0.09) \quad \mathrm{km\,s^{-1}}, \end{aligned} \tag{20}$$

where the possible effect arising from a systematic error of 0.1 mas in the parallax is given in brackets. When we use this value of the

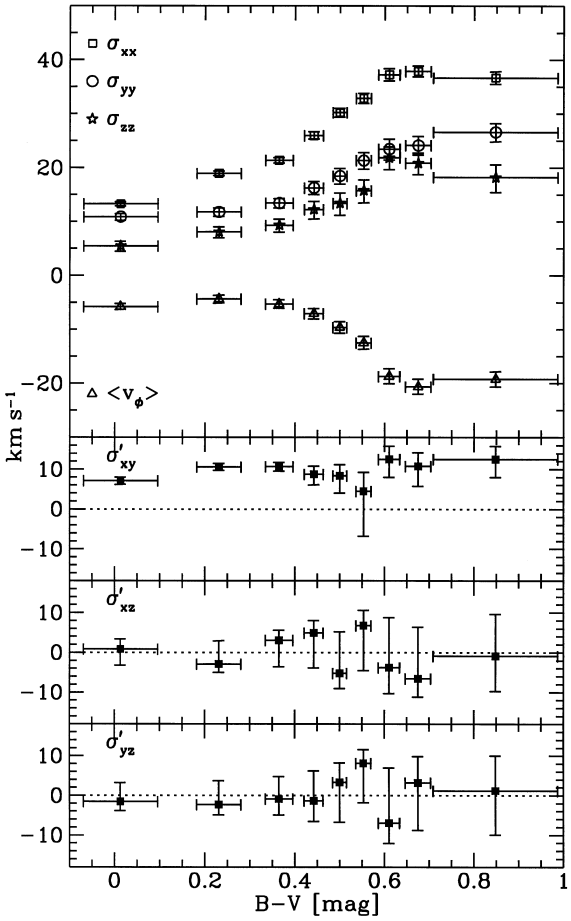

Figure 5. Velocity dispersions for stars in different colour bins. The top panel shows the mean rotation velocity (negative values imply lagging with respect to the LSR) and the three main velocity dispersions. In the three bottom panels $\sigma'_{ij} \equiv \mathrm{sign}(\sigma^2_{ij})\,|\sigma^2_{ij}|^{1/2}$ is plotted for the mixed components of the tensor σ^2_{ij}.

solar motion to calculate values of $\langle v_y \rangle$ relative to the LSR for our stellar groups, Strömberg's asymmetric drift equation is found to be

$$\langle v_y \rangle = -\sigma^2_{xx}/k, \tag{21}$$

where $k = 80 \pm 5\,\mathrm{km\,s^{-1}}$ and we have used $S^2 \simeq 1.14\sigma^2_{xx}$.

4.3 The velocity dispersion tensor

We divided the 11 865 stars of our sample into nine bins in $B-V$ with equal numbers of stars in each bin, and determined $\boldsymbol{\sigma}^2$ as described in Sections 3.3 and 3.4.3. The results are displayed in Fig. 5 and Table 1. The errors correspond to the 15.7 and 84.3 percentiles (1σ error) and have been evaluated via Monte Carlo sampling assuming a multivariate Gaussian distribution in the σ^2_{ij} with variance evaluated via equation (15). In the upper panel of Fig. 5 the three diagonal velocity dispersions and $\langle v_\phi \rangle \equiv \langle v_y \rangle + V_0$ are plotted versus $B-V$. Parenago's discontinuity is visible in all three σ_{ii} and $\langle v_\phi \rangle$, although, owing to the larger bin size, less clearly than in Fig. 3 above. The ordering between the diagonal components of $\boldsymbol{\sigma}^2$ is the same for all colour bins: $\sigma_{xx} > \sigma_{yy} > \sigma_{zz}$.

The lower three panels of Fig. 5 show

$$\sigma'_{ij} \equiv \mathrm{sign}(\sigma^2_{ij})\,\sqrt{|\sigma^2_{ij}|} \tag{22}$$

for the mixed components of the velocity dispersion tensor $\boldsymbol{\sigma}^2$. Evidently, the mixed moments involving vertical motions vanish within their errors. This is to be expected for essentially all possible dynamical configurations of the Milky Way. On the other hand, the mixed dispersion in the plane, σ^2_{xy}, differs significantly from zero, which is not allowed in a well-mixed axisymmetric Milky Way. Thus the principal axes of $\boldsymbol{\sigma}^2$ are not aligned with our Cartesian coordinate frame. We diagonalized the tensor $\boldsymbol{\sigma}^2$ to obtain its eigenvalues σ^2_i. The square root of the largest of these as well as the ratios to the smaller ones are given in Table 1. The ratio $\sigma_1/\sigma_2 \simeq 1.6$, whereas $\sigma_1/\sigma_3 \simeq 2.2$ with a trend for smaller values at redder colours.

Also given in Table 1 is the 'vertex deviation', commonly used to parametrize the deviation from dynamical symmetry. This is

Table 1. Eigenvalues of $\boldsymbol{\sigma}^2$ for the nine colour bins and all stars beyond Parenago's discontinuity (last row).

bin	$(B-V)$	min, max	σ_1	σ_1/σ_2	σ_1/σ_3	ℓ_v
1	−0.238	0.139	$14.35^{+0.49(0.20)}_{-0.40(0.15)}$	$1.52^{+0.16}_{-0.14}$	$2.63^{+0.94}_{-0.28}$	$30.2^{+4.7}_{-5.3}$
2	0.139	0.309	$20.17^{+0.50(0.20)}_{-0.43(0.20)}$	$2.11^{+0.13}_{-0.28}$	$2.51^{+0.83}_{-0.10}$	$22.8^{+2.8}_{-3.0}$
3	0.309	0.412	$22.32^{+0.56(0.15)}_{-0.47(0.18)}$	$1.89^{+0.14}_{-0.20}$	$2.40^{+0.66}_{-0.14}$	$19.8^{+3.2}_{-3.4}$
4	0.412	0.472	$26.26^{+0.80(0.21)}_{-0.59(0.01)}$	$1.66^{+0.12}_{-0.15}$	$2.16^{+0.52}_{-0.15}$	$10.2^{+5.0}_{-5.4}$
5	0.472	0.525	$30.37^{+0.96(0.22)}_{-0.70(0.21)}$	$1.66^{+0.13}_{-0.15}$	$2.28^{+0.77}_{-0.18}$	$6.9^{+5.1}_{-5.3}$
6	0.525	0.582	$32.93^{+1.09(0.22)}_{-0.75(0.21)}$	$1.51^{+0.13}_{-0.12}$	$2.19^{+0.64}_{-0.19}$	$1.9^{+6.0}_{-6.1}$
7	0.582	0.641	$37.64^{+1.37(0.23)}_{-0.94(0.23)}$	$1.61^{+0.07}_{-0.18}$	$1.78^{+0.48}_{-0.04}$	$10.2^{+5.6}_{-6.0}$
8	0.641	0.719	$38.13^{+0.71(0.23)}_{-0.31(0.22)}$	$1.60^{+0.10}_{-0.15}$	$1.84^{+0.42}_{-0.08}$	$7.6^{+5.9}_{-6.0}$
9	0.719	1.543	$37.20^{+1.41(0.16)}_{-0.93(0.15)}$	$1.44^{+0.12}_{-0.12}$	$2.04^{+0.61}_{-0.16}$	$13.1^{+6.7}_{-7.6}$
—	0.610	1.543	$37.91^{+0.79(0.20)}_{-0.63(0.20)}$	$1.54^{+0.07}_{-0.09}$	$1.86^{+0.21}_{-0.08}$	$10.3^{+3.9}_{-3.9}$

$\sigma_1, \sigma_2, \sigma_3$ are the roots of the largest, middle and smallest eigenvalues of the velocity dispersion tensor $\boldsymbol{\sigma}^2$. ℓ_v is the vertex deviation (equation 23). Units are mag, $\mathrm{km\,s^{-1}}$ and degrees for $B-V$, σ_i and ℓ_v respectively. The errors given correspond to the 15.7 and 84.3 percentiles, i.e. 1σ error. The maximum deviations resulting from a systematic error of 0.1 mas in the parallaxes are given in brackets (only for σ_1; for all other quantities listed the deviations are neglible compared with the uncertainties).

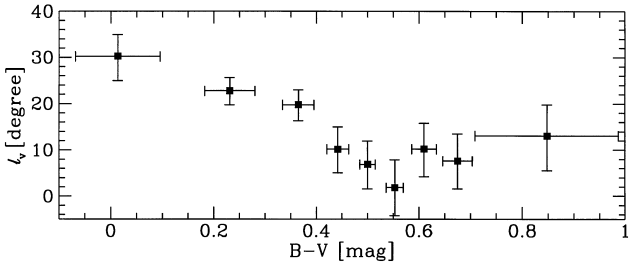

Figure 6. The vertex deviation ℓ_v versus $B-V$ colour. The error bars correspond to the 15.7 and 84.3 percentiles (i.e. 1σ error) and have been obtained assuming a multivariate Gaussian distribution in the σ_{ij}^2 with variance evaluated via equation (15).

defined to be

$$\ell_v \equiv \tfrac{1}{2}\arctan\left(\frac{2\sigma_{xy}^2}{\sigma_{xx}^2-\sigma_{yy}^2}\right), \tag{23}$$

and is the angle by which one has to rotate our Cartesian coordinate system around its $\hat{z}$ axis such that the resulting velocity dispersion tensor is diagonal in the $v_x v_y$ plane. Hence ℓ_v is the Galactic longitude of the direction of σ_1^2, the largest eigenvalue of the velocity dispersion tensor. Fig. 6 shows ℓ_v as a function of colour. Blueward of Parenago's discontinuity, there is a clear trend of ℓ_v decreasing with $B-V$. Redward of Parenago's discontinuity, stellar kinematics is independent of $B-V$ and it makes sense to group all 3330 stars into a single bin. The results are given in the last row of Table 1. The hypothesis that $\ell_v \le 0$ for this group of stars is excluded at the 99.5 per cent confidence level.[1]

5 DISCUSSION

We have analysed a kinematically unbiased sample of nearly 12 000 main-sequence stars for which the *Hipparcos* satellite measured parallaxes that have errors smaller than 10 per cent. From this sample we have re-determined most of the key kinematic parameters of the solar neighbourhood with unprecedented accuracy.

On account of the unusually small accidental and systematic errors of the *Hipparcos* data, our errors are dominated by Poisson noise; we are characterizing the distribution of stars in three-dimensional velocity space from samples of typically 500 stars. From this fact it follows that our error estimates may be considered reliable.

Equation (20) gives the velocity of the Sun with respect to the LSR. In common with several recent studies (Mayor 1974; Gomez & Messenier 1977; Oblak 1983; Bienaymé & Sechaud 1997) this has a smaller azimuthal component ($V_0 = 5.2 \pm 0.6\,\mathrm{km\,s^{-1}}$) than Delhaye's (1965) classical value, $12\,\mathrm{km\,s^{-1}}$. A contributory factor to this discrepancy is probably the fact that stars bluer than $B-V \simeq 0$ have anomalous values of both $\langle v_x \rangle$ and $\langle v_y \rangle$, presumably because they are not yet well mixed. We have ignored such stars in our determination of the Sun's motion with respect to the LSR.

Equation (21) quantifies the asymmetric drift. As is well known, the coefficient k that occurs in it constrains the radial gradients of stellar density and the velocity dispersion tensor, $\boldsymbol{\sigma}^2$. Quantitatively, if R_d is the scalelength of the disc, and ν the mid-plane stellar density, with equation (4-34) of BT we may infer from equation (21) that

$$\frac{R_0}{R_d} \simeq -\tfrac{1}{2}\frac{\partial \ln \nu\sigma_{xx}^2}{\partial \ln R}\bigg|_{R_0} = \frac{v_c}{k} + \tfrac{1}{2}\left[1-\frac{\sigma_{yy}^2}{\sigma_{xx}^2} \dot{+} \left(1-\frac{\sigma_{zz}^2}{\sigma_{xx}^2}\right)\right] \simeq 3.0 \dot{+} 0.4. \tag{24}$$

Here the first equality involves the assumption that $\sigma_{xx}^2 \propto \nu$, which is based on the observation that disc scaleheights vary little with radius, and the term that follows the symbol $\dot{+}$ may or may not be required, depending on whether the longest axis of $\boldsymbol{\sigma}^2$ points to the Galactic Centre or remains horizontal as one moves above the plane [cf. section 4.2.1(a) of BT]. The numerical values given are based on Table 1, $R_0 = 8\,\mathrm{kpc}$ and the Feast & Whitelock values of the Oort constants. The relatively short scalelength implied by equation (24) is consistent with recent infrared-based studies of the Galaxy (Kent, Dame & Fazio 1991; Malhotra et al. 1997).

The shape of the velocity ellipsoid does not vary significantly with $B-V$; to within the errors its axial ratios are constant at $\sigma_1/\sigma_3 \simeq 2.2$ and $\sigma_1/\sigma_2 \simeq 1.6$. The ratio $\sigma_{yy}^2/\sigma_{xx}^2 \simeq 0.4$ is intimately connected with the values of the Oort constants, being naïvely given by Oort's equation $-B/(A-B) \simeq 0.45$. Unfortunately, Oort's relation is significantly in error for typical star samples (Binney 1986), but Cuddeford & Binney (1994) argue that $-B/(A-B)$ can be accurately determined from $\sigma_{yy}^2/\sigma_{xx}^2$ if modified rather than normal moments are employed. We hope soon to evaluate these modified moments from the present sample.

The ratio σ_1/σ_3 constrains the nature of the scattering process that is responsible for the increase in stellar velocity dispersion with age (e.g. Jenkins 1992). The value determined here is consistent with previous values, and implies that both spiral structure and scattering by molecular clouds contribute significantly to heating of the local disc. We find a hint of smaller values of σ_1/σ_3 for redder colours, which is the trend expected if heating by spiral structure is less efficient relative to cloud scattering for dynamically hotter stellar populations.

We have shown that one principal axis of the velocity ellipsoid coincides with the direction $b = 90°$. The angle by which the longest axis of the velocity ellipsoid deviates from the direction to the Galactic Centre, the vertex deviation ℓ_v, decreases from large values ($\ell_v \gtrsim 20°$) for early types up to the colour of Parenago's discontinuity, and is then consistent with being constant at $\ell_v \simeq 10°$.

Two factors probably contribute to the vertex deviation: (i) the likelihood that a significant fraction of young stars belong to a small number of moving groups, and (ii) any large-scale non-axisymmetric component in the Galactic potential, such as would be generated by either a bar or spiral structure. Spiral arms will contribute to the vertex deviations of all stellar groups, but their contribution will be largest for the populations with the smallest velocity dispersions, because stars with epicycle amplitudes comparable to or larger than the inter-arm spacing will respond weakly to the spiral's potential. Hence the more tightly wound the arms are, the more strongly the effect will be confined to the earlier spectral types. The fact that we see a significant vertex deviation to the latest spectral types implies that the causative agent is either a bar or rather open spiral arms. To quantify this point, let X be the epicycle amplitude of a typical late-type star. Then the star's radius is $R(t) = R_g + X\cos(\kappa t)$, where $\kappa = 2\sqrt{B^2 - AB} \simeq 36.7\,\mathrm{km\,s^{-1}\,kpc^{-1}}$ is the epicycle frequency and R_g the guiding centre of the star. To a reasonable approximation we may equate the time average of $\dot{R}^2$ to $\sigma_1^2 \simeq (38\,\mathrm{km\,s^{-1}})^2$. Hence $X \simeq \sqrt{2}\sigma_1/\kappa \simeq 1.5\,\mathrm{kpc}$ and the star

[1] It is important to bear in mind that the errors in ℓ_v are not distributed as a Gaussian.

moves ~ 3 kpc in each epicycle period. We would not expect spiral arms with inter-arm spacing $\Delta \lesssim 3$ kpc to have much effect on the orbit of such a star. It is clearly important to quantify this interesting conclusion more precisely. Kuijken & Tremaine (1991) give an estimate of the magnitude of the vertex deviation that would be generated by a component of the Galaxy's gravitational potential proportional to $\exp[\mathrm{i}(m\phi - \omega t)]$.

Finally it seems worth remarking that, in characterizing the distribution of stars in velocity space by its first few moments, we in no way imply that the distribution is similar to Schwarzschild's ellipsoidal distribution, as given, for example, by equation (7-91) of BT; the velocity ellipsoid is a formal construct which need have no physical counterpart. From these data it *is* possible to map the distribution of stars in velocity space and discover how closely it resembles Schwarzschild's paradigm, but that topic is reserved for a future paper (Dehnen 1998).

REFERENCES

Barbanis B., Woltjer L., 1967, ApJ, 150, 461

Bienaymé O., Sechaud N., 1997, A& A, 323, 781

Binney J. J., 1986, in Gilmore G., Carswell R., eds, The Galaxy. Reidel, Dordrecht, p. 399

Binney J. J., Lacey C. G., 1988, MNRAS, 230, 597

Binney J. J., Temaine S., 1987, Galactic Dynamics. Princeton Univ. Press, Princeton, NJ (BT)

Binney J. J., Dehnen W., Houk N., Murray C. A., Penston M. J., 1997, in Perryman M. A. C., ed., The *Hipparcos* Venice Symposium 1997. ESA SP-402, p. 473

Dehnen W., 1998, AJ, in press

Delhaye J., 1965, in Blaauw A., Schmidt M., eds, Stars and Stellar Systems, Vol. 5. Univ. Chicago Press, Chicago, p. 61

Cuddeford P., Binney J. J., 1994, MNRAS, 266, 273

ESA, 1997, The *Hipparcos* and Tycho Catalogues, ESA SP-1200

Feast M. W., Whitelock P. A., 1997, MNRAS, 291, 683

Gomez A., Messenier M. O., 1977, A& A, 54, 113

Houk N., 1978, Catalogue of Two-Dimensional Spectral Types for the HD Stars, Vol. 2. Dept. of Astronomy, Univ. of Michigan, Ann Arbor

Houk N., 1982, Catalogue of Two-Dimensional Spectral Types for the HD Stars, Vol. 3. Dept. of Astronomy, Univ. of Michigan, Ann Arbor

Houk N., Cowley A. P., 1975, Catalogue of Two-Dimensional Spectral Types for the HD Stars, Vol. 1. Dept. of Astronomy, Univ. of Michigan, Ann Arbor

Jenkins A., 1992, MNRAS, 257, 620

Kent S. M., Dame T. M., Fazio G., 1991, ApJ, 378, 131

Kuijken K., Tremaine S., 1991, in Sundelius B., ed., Dynamics of Disk Galaxies. Göteborg University Press, Göteborg, p. 71

Malhotra S., Spergel D. N., Rhoads J. E., Li J., 1996, ApJ, 473, 687

Mayor M., 1974, A& A, 32, 321

Oblak E., 1983, A& A, 123, 238

Parenago P. P., 1950, AZh, 27, 150

Roman N. G., 1950, ApJ, 112, 554

Roman N. G., 1952, ApJ, 116, 122

Schwarzschild K., 1908, Nachr. Kgl. Ges. d. Wissenschaften, Göttingen, p. 191

Spitzer L., Schwarzschild M., 1953, ApJ, 118, 106

Wielen R., 1977, A&A, 60, 263

This paper has been typeset from a $\mathrm{T_EX/L^AT_EX}$ file prepared by the author.